lubricants

MDPI

Review

Molecular Dynamics Simulation on Polymer Tribology: A Review

Tianqiang Yin [1], Guoqing Wang [1], Zhiyuan Guo [1], Yiling Pan [1], Jingfu Song [2], Qingjun Ding [1] and Gai Zhao [1,*]

[1] State Key Laboratory of Mechanics and Control for Aerospace Structures, Nanjing University of Aeronautics and Astronautics, Nanjing 210016, China; tianqiangyin@nuaa.edu.cn (T.Y.); wangguoqing@nuaa.edu.cn (G.W.); guozhiyuan@nuaa.edu.cn (Z.G.); panyiling@nuaa.edu.cn (Y.P.); dingqingjun@nuaa.edu.cn (Q.D.)

[2] School of Naval Architecture & Ocean Engineering, Jiangsu Maritime Institute, Nanjing 211170, China; songjingfu1984@126.com

* Correspondence: zhaogai@nuaa.edu.cn

Abstract: A profound comprehension of friction and wear mechanisms is essential for the design and development of high-performance polymeric materials for tribological application. However, it is difficult to deeply investigate the polymer friction process in situ at the micro/mesoscopic scale by traditional research methods. In recent years, molecular dynamics (MD) simulation, as an emerging research method, has attracted more and more attention in the field of polymer tribology due to its ability to show the physicochemical evolution between the contact interfaces at the atomic scale. Herein, we review the applications of MD in recent studies of polymer tribology and their research focuses (e.g., tribological properties, distribution and conformation of polymer chains, interfacial interaction, frictional heat, and tribochemical reactions) across three perspectives: all-atom MD, reactive MD, and coarse-grained MD. Additionally, we summarize the current challenges encountered by MD simulation in polymer tribology research and present recommendations accordingly, aiming to provide several insights for researchers in related fields.

Keywords: polymer tribology; molecular dynamics simulation; friction and wear mechanisms; atomic scale

check for updates

Citation: Yin, T.; Wang, G.; Guo, Z.; Pan, Y.; Song, J.; Ding, Q.; Zhao, G. Molecular Dynamics Simulation on Polymer Tribology: A Review. *Lubricants* **2024**, *12*, 205. https://doi.org/10.3390/lubricants12060205

Received: 1 April 2024
Revised: 30 May 2024
Accepted: 1 June 2024
Published: 4 June 2024

Correction Statement: This article has been republished with a minor change. The change does not affect the scientific content of the article and further details are available within the backmatter of the website version of this article.

Copyright: © 2024 by the authors. Licensee MDPI, Basel, Switzerland. This article is an open access article distributed under the terms and conditions of the Creative Commons Attribution (CC BY) license (https://creativecommons.org/licenses/by/4.0/).

1. Introduction

Polymers and their composites are widely recognized as excellent friction materials due to their unique physicochemical properties, such as good self-lubrication, high chemical stability, and high wear resistance [1–3]. Because of the designability of their tribological properties, these friction materials can be customized to meet the needs of applications under specific conditions (e.g., high/low temperature, vacuum, and high humidity) by adjusting their molecular structure and species composition [4,5]. However, this design often relies on extensive experimental studies (e.g., material preparation, friction testing, and friction and wear mechanism analysis), making it very labor-intensive and costly [6]. This has significantly limited the development of the field of polymer tribology.

In recent years, molecular dynamics (MD) simulation, as an emerging research tool, has become increasingly significant in industrial applications (e.g., drug design, electrolyte configuration, and construction of other novel materials) and the development of polymeric materials, especially, polymers with low friction coefficient [7–11]. It can generate atomic trajectories by solving Newton's equations of motion using a finite difference scheme over a series of short time steps. Based on this, one can analyze the physicochemical transformations of friction interfaces and predict the tribological properties of new materials at the microscopic scale, thus guiding the related research and development works [12,13]. This plays a significant role in reducing the cost of experiments as well as the consumption of resources.

This paper first provides a brief overview of three dominant MD simulation methods: all-atom MD, reactive MD, and coarse-grained MD, as applied to the study of polymer tribology. Then, the information that can be characterized by these methods is listed, revealing friction and wear mechanisms. Finally, the current challenges faced by MD simulation in polymer tribology research are presented, along with feasible recommendations based on the review. The purpose of this review is to provide polymer tribology researchers interested in MD with a more comprehensive understanding of the unique role of MD simulation.

2. Three Main MD Research Methods and Their Force Field Used in Polymer Tribology

For different research purposes, there are three main research methods for MD simulation. Firstly, all-atom MD simulation, this method considers the interactions between polymer molecules (including van der Waals and Coulomb interactions, etc.) and the interactions within the polymer molecules (such as stretching of bonds, bending of angles, and torsion of dihedrals, etc.). It is mainly used to analyze the physical interactions during the friction process and to predict the properties of materials. Secondly, reactive MD simulation, unlike all-atom MD simulation, allows for bond breaking and formation during the simulation and is, therefore, more often applied to the analysis of tribochemical reactions. Thirdly, when comparing coarse-grained MD simulation with the previous two, the most significant difference lies in the ability to simulate the molecular evolution process in larger spatial and temporal scales (i.e., from nanometers to microns on the spatial scale, and from femtoseconds to microseconds or even milliseconds on the time scale) [14], which is of great importance for the design and investigation of polymer composites. These three methods are briefly discussed below.

2.1. All-Atom MD Simulation

The core of all-atom MD simulation is the force field; the simulations based on different force fields may have differences in the results, so the selection of appropriate force fields for different research objects is crucial for all-atom MD simulation. From the relevant literature in the field of polymer tribology in recent years [6,12,13], the following four force fields are the most utilized.

2.1.1. COMPASS Force Filed

The COMPASS (condensed-phase optimized molecular potentials for atomistic simulation studies) force field is currently the most widely used in MD simulation studies of polymer tribology [15]. It is designed to simulate common organic molecules, inorganic small molecules, and polymers. This force field was developed based on a consistent force field (CFF)-type force field with optimized nonbond parameters. Its specific functional form is as follows:

$$E_{total} = E_{valence} + E_{nonbond} \quad (1)$$

where the valence energy ($E_{valence}$) consists of bond energy (E_{bond}), angle energy (E_{angle}), torsion angle energy ($E_{torsion}$), out of plane angle energy (E_{OOPA}), and cross-coupling energy (E_{cross}) including combinations of two or three internal energies.

$$\begin{aligned} E_{valence} &= E_{bond} + E_{angle} + E_{torsion} + E_{OOPA} + E_{cross} \\ &= \sum_{bond}\left[k_2(b-b_o)^2 + k_3(b-b_o)^3 + k_4(b-b_o)^4\right] \\ &+ \sum_{angel}\left[k_2(\theta-\theta_o)^2 + k_3(\theta-\theta_o)^3 + k_4(\theta-\theta_o)^4\right] \\ &+ \sum_{torsion}[k_1(1-cos\phi) + k_2(1-cos2\phi) + k_3(1-cos3\phi)] \\ &+ \sum_{OOPA} k_2\chi^2 \\ &+ \sum_{bond,bond} k(b-b_o)(b'-b'_o) \\ &+ \sum_{bond,angle} k(b-b_o)(\theta-\theta_o) \\ &+ \sum_{bond,torsion} (b-b_o)[k_1 cos\phi + k_2 cos2\phi + k_3 cos3\phi] \\ &+ \sum_{angle,torsion} (\theta-\theta_o)[k_1 cos\phi + k_2 cos2\phi + k_3 cos3\phi] \\ &+ \sum_{angle,angle} k(\theta'-\theta'_o)(\theta-\theta_o) \\ &+ \sum_{angle,angle,torsion} k(\theta-\theta_o)(\theta'-\theta'_o)cos\phi \end{aligned} \quad (2)$$

In Equation (2), k is the force constant, b and θ are the bond and angle parameters. The nonbond energy includes the Lennard–Jones potential (for van der Waals interactions) and the Coulomb term (for electrostatic interactions), as follows:

$$E_{nonbond} = \sum_{i,j}\epsilon_{ij}\left[2\left(\frac{r^o_{ij}}{r_{ij}}\right)^9 - 3\left(\frac{r^o_{ij}}{r_{ij}}\right)^6\right] + \sum_{i,j}\frac{q_i q_j}{r_{ij}} \quad (3)$$

In recent years, the developers of the COMPASS force field have expanded and optimized it, developing COMPASS II (broadening support for polymer and drug-like molecules) and COMPASS III (adding support for ionic liquids). This further enhances the usefulness of the COMPASS force field in polymer tribology studies [16,17].

2.1.2. CVFF Force Field

The CVFF (consistent valence force field) was developed by Dauber–Osguthorpe group [18]. It was initially used to simulate small organic molecules and proteins, and it has been extended to apply to certain inorganic systems, such as silicates, aluminosilicates, and phosphosilicon compounds. Its functional form is given below:

$$\begin{aligned} E_{total} &= \sum_b D_b(b-b_o)^2 + \sum_\theta H_\theta(\theta-\theta_o)^2 + \sum_\phi H_\phi[1+s\cos(n\phi)] + \sum_\chi H_\chi\chi^2 \\ &+ \sum_b\sum_{b'} F_{bb'}(b-b_o)(b'-b'_o) + \sum_\theta\sum_{\theta'} F_{\theta\theta'}(\theta-\theta_o)(\theta'-\theta'_o) \\ &+ \sum_b\sum_\theta F_{b\theta}(b-b_o)(\theta-\theta_o) + \sum_\phi F_{\phi\theta\theta'}cos\phi(\theta-\theta_o)(\theta'-\theta'_o) \\ &+ \sum_\chi\sum_{\chi'} F_{\chi\chi'}\chi\chi' + \sum\epsilon\left[\left(\frac{r^*}{r}\right)^{12} - 2\left(\frac{r^*}{r}\right)^6\right] + \sum\frac{q_i q_j}{\epsilon r_{ij}} \end{aligned} \quad (4)$$

The composition of the CVFF function is similar to that of the COMPASS force field. The first four terms of Equation (4) represent harmonic contributions of stretching and compression for bonds, of valence angle bending, of internal rotation or torsion for dihedral angle, and of (out-of-plane) improper angles, respectively. The next five terms are related to cross-interactions. And the last two items indicate van der Waals and Coulomb interactions, respectively. Currently, due to the good compatibility of this force field for organic systems, results in favorable agreement with the experiment have been obtained when used in polymer tribology studies, but further generalization of this force field is limited by the fact that its parameter library is not comprehensive [19–21].

2.1.3. PCFF Force Field

The PCFF (polymer consistent force field) was developed from the CFF91-type force field and has been applied mainly to the simulations of polymers and organic materials; its functional form is as follows [22,23]:

$$\begin{aligned} E_{total} &= \sum \sum_{n=2}^{4} k_n^b (b-b_0)^n + \sum \sum_{n=2}^{4} k_n^a (\theta-\theta_0)^n + \sum \sum_{n=1}^{3} k_n^t (1-cosn\phi) \\ &+ \sum k^{(0)} (\chi-\chi_0)^2 + \sum k^{bb'} (b-b_0)(b'-b_0') + \sum k^{ba} (b-b_0)(\theta-\theta_0) \\ &+ \sum k^{aa'} (\theta-\theta_0)(\theta'-\theta_0') + \sum \sum_{n=1}^{3} k_n^{bt} (b-b_0) cosn\phi \\ &+ \sum \sum_{n=1}^{3} k_n^{at} (\theta-\theta_0) cosn\phi + \sum k^{aa't} (\theta-\theta_0)(\theta'-\theta_0') cos\phi \\ &+ \sum \epsilon \left[2\left(\frac{r^*}{r}\right)^9 - 3\left(\frac{r^*}{r}\right)^6 \right] + \sum \frac{q_i q_j}{r_{ij}} \end{aligned} \tag{5}$$

As shown in Equation (5), the total energy contains contributions from intramolecular (bonded) interactions as well as from intermolecular (nonbonded) interactions. This is similar to the COMPASS force field as they are both developed based on CFF-type force fields.

2.1.4. OPLS-AA Force Field

The OPLS-AA (all-atom optimized potentials for liquid simulations) force field was developed by the Jorgensen group, and is mainly used to calculate the physical properties of condensed matter [24]. The force field does not consider the cross-coupling terms, and its functional form is as follows:

$$\begin{aligned} E_{total} &= \sum_i k_{b,i} (r_i - r_{o,i})^2 + \sum_i k_{\theta,i} (\theta_i - \theta_{o,i})^2 + \sum_i \left[\frac{1}{2} V_{1,i} (1 + cos\phi) \right. \\ &\left. + \frac{1}{2} V_{2,i} (1 - cos2\phi) + \frac{1}{2} V_{3,i} (1 + cos3\phi) + \frac{1}{2} V_{4,i} (1 - cos4\phi) \right] \\ &+ \sum_i \sum_{j>i} \left\{ 4\varepsilon_{ij} \left[\left(\frac{\sigma_{ij}}{r_{ij}}\right)^{12} - \left(\frac{\sigma_{ij}}{r_{ij}}\right)^6 \right] + \frac{q_i q_j e^2}{r_{ij}} \right\} \end{aligned} \tag{6}$$

with the combining rules:

$$\sigma_{ij} = \sqrt{\sigma_{ii}\sigma_{jj}} \tag{7}$$

$$\varepsilon_{ij} = \sqrt{\varepsilon_{ii}\varepsilon_{jj}} \tag{8}$$

Because the nonbond parameters of this force field are derived from quantum chemical computational results and the fitting of experimental data, it works well in the simulations of condensed-phase systems. Hence, it is popular in studies of polymer materials [25–27].

2.2. Reactive MD Simulation

Classical MD simulation based on all-atom force fields generally disallow bond breaking and formation. Therefore, it is not capable of simulating chemical reactions. To deal with this deficiency, researchers have developed the reactive force field (ReaxFF) [28]. It employs a bond-order formalism in conjunction with polarizable charge descriptions to describe both reactive and non-reactive interactions between atoms. This allows ReaxFF to describe the physical/chemical interactions between a diverse range of materials accurately. The composition of this force field function is as follows [29,30]:

$$E_{system} = E_{bond} + E_{over} + E_{angle} + E_{tors} + E_{vdWaals} + E_{Coulomb} + E_{Specific} \tag{9}$$

E_{bond}, E_{angle}, and E_{tors} are associated with bond energy, angle energy, and torsion angle energy, respectively, which is similar to the all-atom force field. E_{over} is an energy penalty

preventing the over coordination of atoms, which is based on atomic valence rules (e.g., a stiff energy penalty is applied if a carbon atom forms more than four bonds). The van der Waals and Coulomb interactions between atoms are determined by parameters $E_{vdwaals}$ and $E_{Coulomb}$. $E_{Specific}$ represents some specific properties present in the studied system, such as lone-pair, conjugation, hydrogen binding, etc. Full functional forms can be found in reference [31].

2.3. Coarse-Grained MD Simulation

MD simulation is usually performed at the nanoscale due to the limitation of the current computility. At this point, the polymer polymerization degree is usually no more than 10^2. In practice, a lot of polymers have a polymerization degree of more than 10^3 or even 10^4, which may make it difficult to match the simulated results with the experimental ones [32]. Coarse-grained MD simulation, as a method derived from classical MD simulation, calculates the evolution of molecules at larger scales (i.e., bringing simulation closer to reality) by mapping multiple atoms or groups into a coarse-grained "particle". Generally, the construction of the coarse-grained system consists of two aspects: (1) building mapping relationships; (2) establishing the coarse-grained force field. The former is directly related to the computational efficiency of coarse-grained MD; a reasonable mapping scheme can obtain calculation results at a higher computational rate. Regarding the latter, there are currently two main construction methods [14,33,34]. One is the bottom-up approach, which is based on all-atom simulation to generate coarse-grained force field functions and parameters. The other is to obtain the force field parameters from the top-down, e.g., Martini force field. It considers 3–4 non-hydrogen atoms in common organic molecules as a coarse-grained particle and compares the simulation results with experimental measurements to fit the resultant force field parameters. At present, the Martini force field has been updated to the third generation, with further improvements in the description of hydrogen bonding and electronic polarizability, making it better able to simulate ionic liquids and polymers [35–39].

3. Typical Polymer Tribological Problems Solved by MD Simulation

Friction is a complex physicochemical process. It is not only related to the properties of the friction material itself but also to the interactions between the contact interfaces (e.g., adhesion and tribochemical reactions). With the three types of MD simulation discussed above, we can investigate the physicochemical evolution during the friction from the following three aspects: (1) the mechanical properties of the material itself and the physical interactions during friction; (2) the chemical reactions occurring at the friction interface; and (3) the physical changes during friction at mesoscopic scales. Next, these three aspects are briefly summarized.

3.1. Friction and Wear Mechanisms Revealed by All-Atom MD Simulation

3.1.1. Mechanical Properties

By predicting the mechanical properties (e.g., elastic modulus) of a polymer/polymer composite, the tribological properties of the material can be inferred to some extent [40,41]. Chen et al. calculated the bulk, shear, and Young's modulus of carbon nanotube (CNT)/nitrile butadiene rubber (NBR) composites by the constant-strain method (Figure 1). The results indicated that the increase in acrylonitrile content improved the mechanical properties of the composite at constant CNT content, which is attributed to the polar interactions between the -CN groups [42]. Similarly, the elastic modulus of polymer/polymer composites such as Eucommia ulmoides gum (EUG)/natural rubber (NR), polyamide 66 (PA66)/graphene (GE), and polyimide (PI)/lanthana can be calculated with the assistance of MD simulation [43–45]. This is meaningful for the design of novel polymer friction materials.

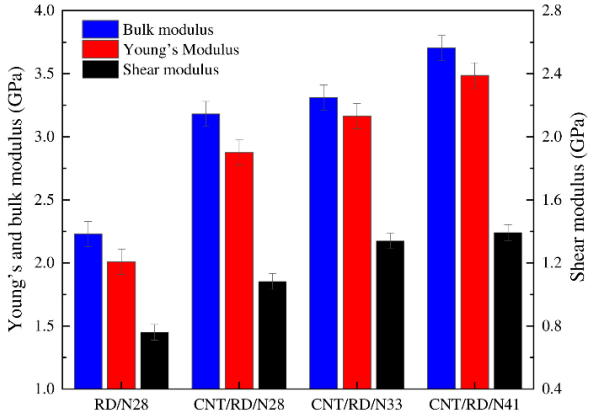


Figure 1. Mechanical properties of NBR composites with various acrylonitrile contents [42].

3.1.2. Free Volumes (FVs)

FV is often used to reflect the compatibility of components within a polymer composite; the smaller the value, the better the compatibility of the polymer with its internal fillers. It can also be presented as a fractional free volume (FFV), as shown in Equation (10):

$$\mathrm{FFV} = \frac{V_f}{V_{total}} = \frac{V_{total} - 1.3V_w}{V_{total}} \tag{10}$$

where V_{total}, V_f, and V_w represent the total volume, the free volume, and the van der Waals volume, respectively [46–48]. To explore the compatibility of different functionalized graphene sheets (GNS) with the NBR matrix, Cui et al. simulated NBR-containing GNS, hydroxylated GNS, carboxylated GNS, and esterified GNS, and the simulation snapshots are shown in Figure 2b–e. The results reflect that the functionalized GNS has stronger interactions with NBR. Moreover, the carboxylated GNS has the best effect in reducing the FV of the NBR matrix due to its smallest FV (Figure 2a). This laterally demonstrates that carboxylated GNSs are a good filler for NBR [49].

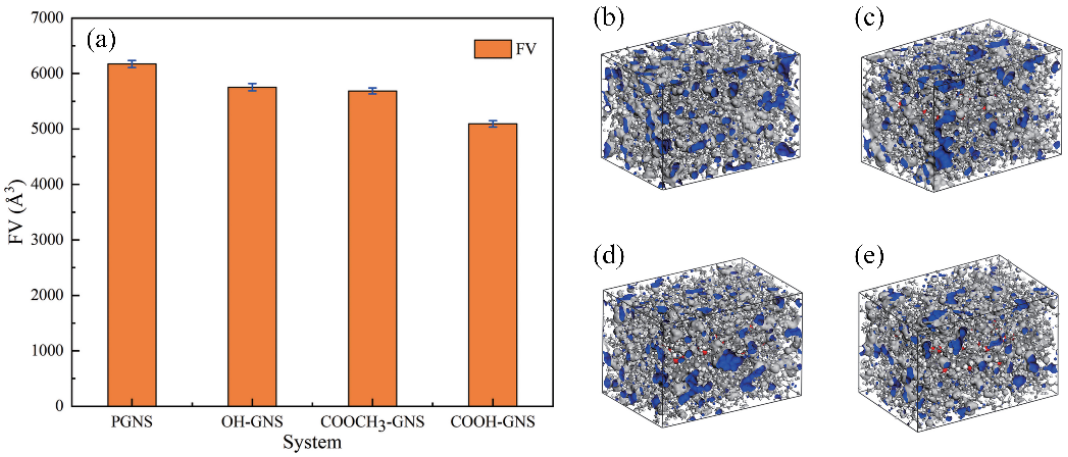


Figure 2. FV of GNS/NBR composites and their snapshots. (**a**) FV. (**b**) PGNS/NBR. (**c**) OH-GNS/NBR. (**d**) $COOCH_3$-GNS/NBR. (**e**) COOH-GNS/NBR [49].

3.1.3. Mean Square Displacement (MSD)

MSD shows the ability of the materials to move and migrate within the polymer matrix; the larger the value, the more the component corresponding to that value has migrated relative to its initial position. MSD is defined as follows:

$$\mathrm{MSD}(t) = \frac{1}{N}\sum_{i=1}^{N} < |r_i(0) - r_i(t)|^2 > \quad (11)$$

where r_i (0) and r_i (t) denote the initial and final positions of the atom at time interval t, respectively. $|r_i$ (0) $- r_i$ (t)$|$ denotes the displacement at time t. N is explained as the number of molecules of the respective component. < > denotes the average of the squared atomic displacements [50–52]. As a common polymer friction material, the adhesion of polytetrafluoroethylene (PTFE) to metal is significant for the comprehension of friction and wear mechanisms. By investigating the MSD of PTFE molecules during PTFE/Fe friction processes, their diffusion motion can be obtained, providing a theoretical basis for analyzing the friction. As shown in Figure 3, Zuo et al. researched the MSD of PTFE molecules under different friction conditions. The simulation results revealed that (1) the α-Fe (110) surface had the strongest interaction with PTFE molecules; (2) the hydroxyl and carbonyl functionalized PTFE was more stable; and (3) PTFE was more prone to adhesion with metal friction pairs at high temperatures [53].

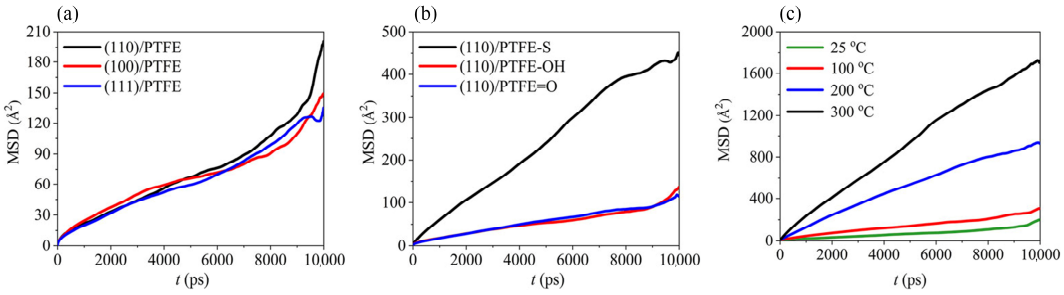


Figure 3. MSD of PTFE molecules under different conditions. (**a**) Fe friction pairs with different crystal structures. (**b**) PTFE molecules with different structures (PTFE-S means chain broken PTFE). (**c**) Different temperature [53]. © 2021 Zuo, Liang, Bao, Yan, Jin and Yang.

3.1.4. Direct Observation of Frictional Interfaces

Unlike macroscopic tribological tests, the friction process performed based on MD simulation can be clearly observed. With the support of several visualization software (e.g., the visualization module in Materials Studio 2024, OVITO 3.10.6, and VMD 1.9.4), it is possible to monitor the deformation, adhesion, and abrasion of the polymer throughout the motion process [54,55]. This helps researchers understand changes between friction contact interfaces at the atomic level [56–60]. Wei et al. found that the wear rate of the composite was greatly reduced due to the adsorption of silica particles on the polymer chains by comparing the microscopic friction process of polyvinyl alcohol (PVA)/polyacrylamide (PAM) with/without filled silica nanoparticles (Figure 4) [61]. Likewise, polymer friction under water-lubricated conditions can be observed. Song et al. investigated the friction process of PTFE/copper under dry friction and water lubrication conditions, as shown in Figure 5. The friction snapshots showed that, relative to dry friction, the wear under water lubrication conditions was drastically reduced because water molecules weaken the adsorption of copper on PTFE molecules [62].

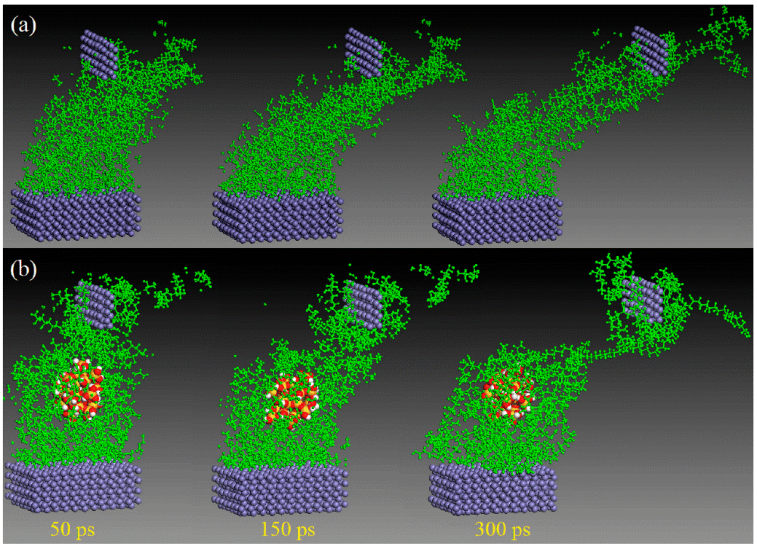


Figure 4. Snapshots of the friction processes (load: 0.12 GPa, velocity: 0.2 Å/ps) of (**a**) the pure PVA/PAM and (**b**) PVA/PAM/silica composites subjected to shear loading by the top Fe layer at different times in MD simulation [61].

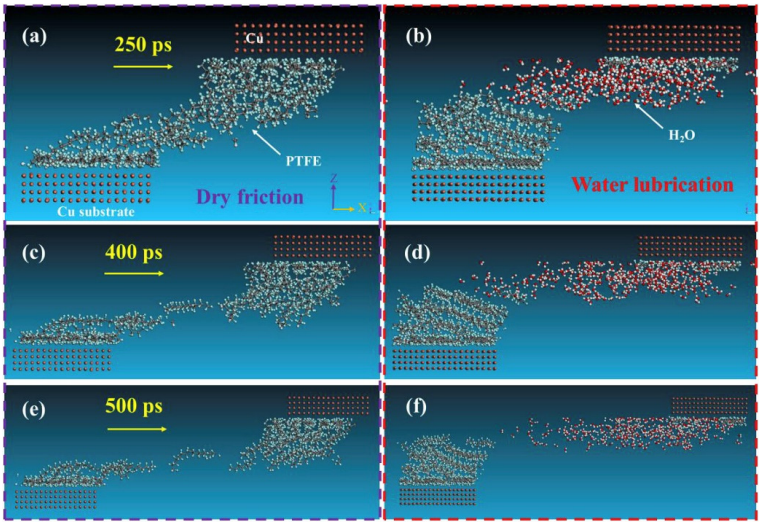


Figure 5. The snapshots of the friction process (load: 1.01 GPa, velocity: 0.1 Å/ps) of the PTFE (**a**,**c**,**e**) under dry friction, and (**b**,**d**,**f**) under water lubrication sliding against Cu layer at 250 ps, 400 ps, 500 ps, respectively [62].

3.1.5. Distribution of Polymer Molecules

It is widely recognized that shearing during friction leads to the rearrangement of polymer molecules near the contact interface, typically resulting in decreased friction and wear. However, the distribution of polymer molecules is difficult to capture experimentally. With the assistance of MD simulation, Wang et al. counted the cosine values of the angle between the C-C bond and the friction direction in different poly α-olefin (PAO) molecules and analyzed their frequencies. The data suggest that syndiotactic PAO molecules with longer carbon chains were more prone to being ordered by the shear effect during the friction process, as indicated by cosine values skewed towards 1 and −1 in Figure 6f. This phenomenon ultimately led to a reduction in frictional resistance [63].

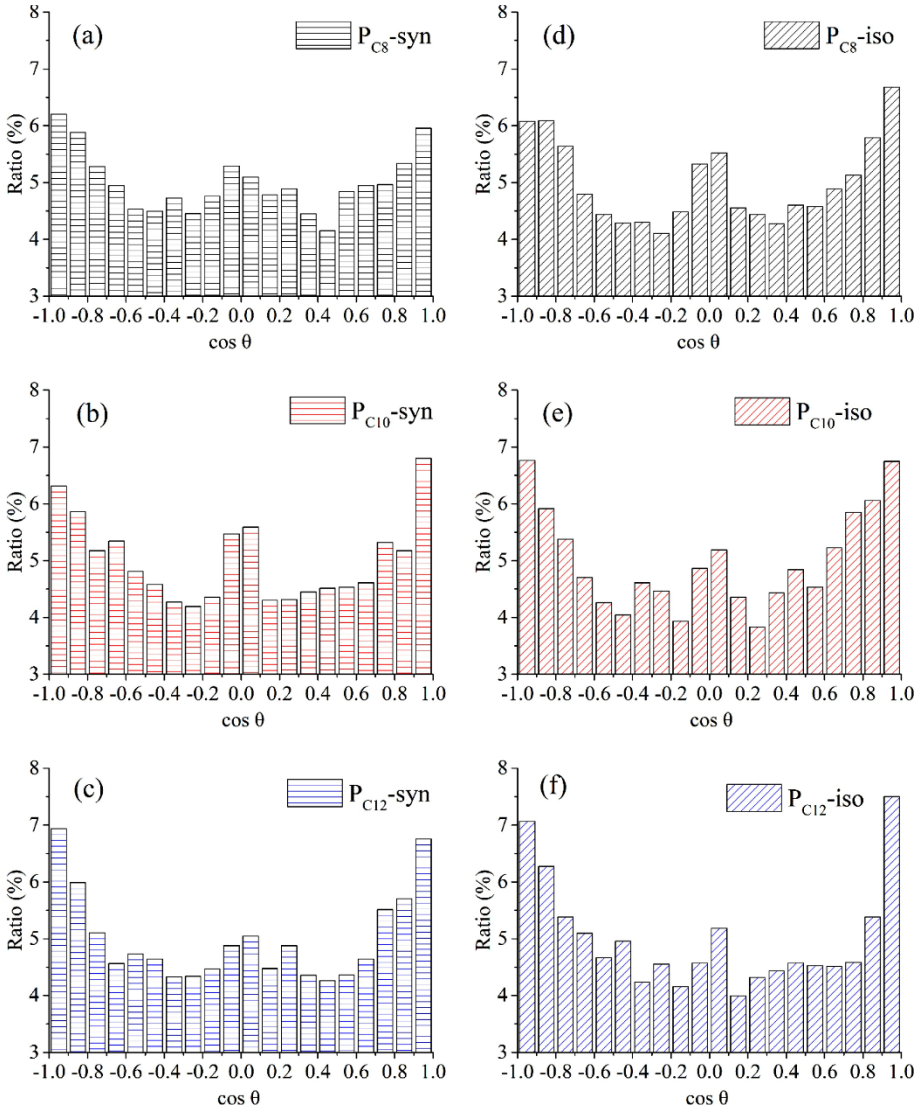


Figure 6. Ordering property of syndiotactic and isotactic PAO molecules after shearing (load: 0.5 GPa, velocity: 0.1 Å/ps). The cosine value of syndiotactic structure is shown in (**a**–**c**). The cosine value of isotactic structure is shown in (**d**–**f**). Black, red, and blue colors represent the carbon chains of PAO containing 8, 10, and 12 carbon atoms, respectively. The more the cosine value of the C-C bond is skewed towards 1 and −1, the more the carbon chain is subjected to shear, i.e., the more it is subjected to shear-thinning, and thus the lower the frictional resistance [63].

The spatial orientation of polymer chains can also be investigated by calculating bond order parameters:

$$S_{ij} = \frac{3}{2} < (e_i \cdot e_j)^2 > -\frac{1}{2} \tag{12}$$

where e_i is the bond unit vector at each atom i, which is calculated from the chord connecting the second neighboring carbon atoms: $e_i = (r_{i+1} - r_{i-1}) / \mid r_{i+1} - r_{i-1} \mid$. And e_j represents the corresponding vector on atom j. Higher S values could be interpreted as increased alignments of polymers, i.e., the increase in crystallinity. Zheng et al. simulated the friction process of copper/amorphous polyethylene (PE) under different loads. They counted the bond order parameters $S(z)$ of PE molecules in the z-direction. The results showed that the friction process under smaller atmospheric pressures favored the ordered arrangement of PE chains, i.e., easier crystallization, as shown in Figure 7 [64,65].

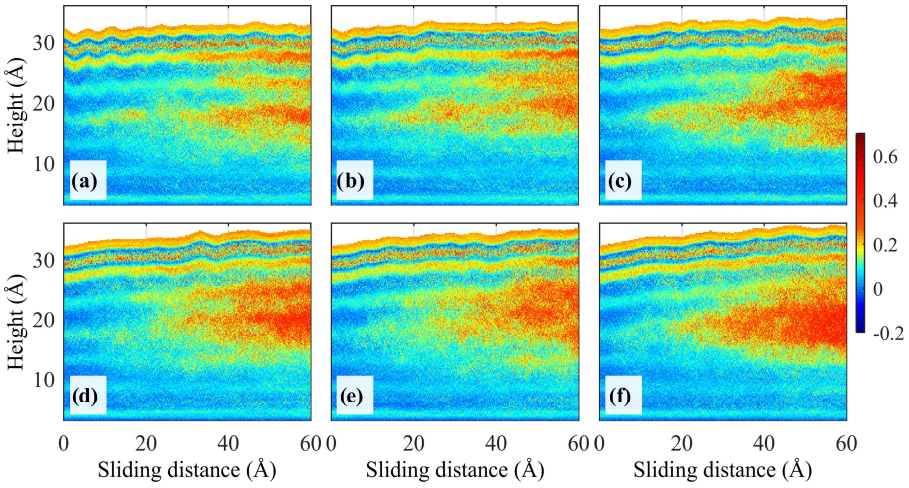


Figure 7. Distribution of the bond order parameters $S(z)$ in the z-direction at v = 40 m/s. (**a**–**f**) P = 70, 50, 30, 10, 5, and 0 MPa [65].

In addition, the density distribution of molecules at the abrasion tracks contributes to the understanding of the mechanism by which pressure affects friction. Figure 8 shows a cross-section of the abrasion tracks left by a copper ball on GNS-coated (flat and crumpled, respectively) PE. We can see that regular high-density lines appear directly below the abrasion tracks, which indicates a local reorganization of the polymer chains. Furthermore, a comparison between Figure 8a,c reveals that a flat GNS is more conducive to reducing the local pressure [66].

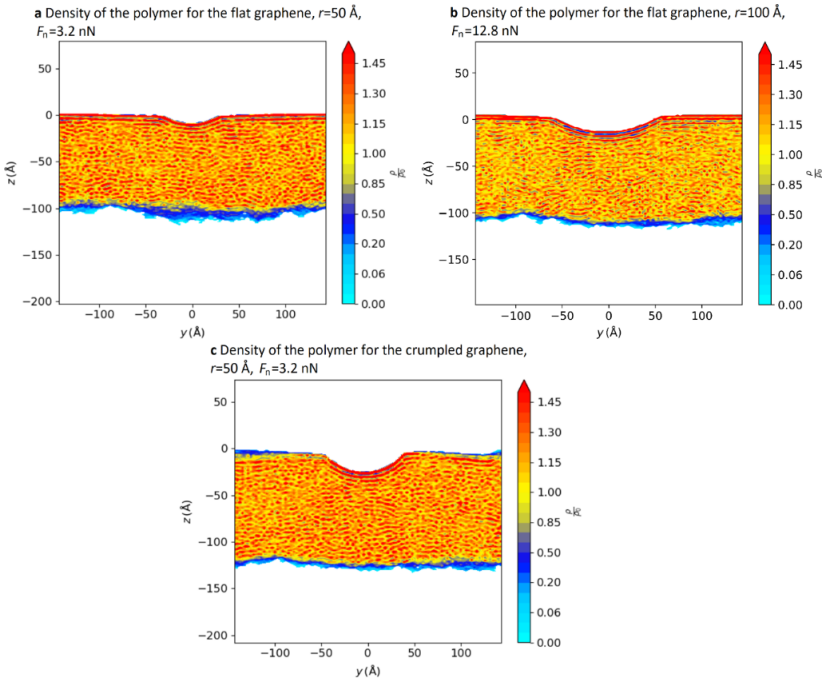


Figure 8. Density maps of the polymer for (**a**) the flat GNS with r = 50 Å and F_n = 3.2 nN, (**b**) the flat graphene sheet with r = 100 Å and F_n = 12.8 nN, and (**c**) the crumpled graphene sheet with r = 50 Å and F_n = 3.2 nN [66]. © 2022 Vacher and de Wijn; licensee Beilstein-Institut.

Similarly, the relative concentration distribution (i.e., number density distribution) is a method of analyzing the distribution of atoms/molecules in space; based on this analysis, it is straightforward to recognize the interaction of atoms/molecules between friction interfaces [67–70]. Qu et al. simulated the friction process of PTFE before and after thermal-

oxidative aging. By analyzing the changes in the relative concentration distribution of PTFE, they found that PTFE was more likely to interact with the metal friction pairs after thermal-oxidative aging (as shown in Figure 9, the concentration of PTFE at the interface is higher after thermal-oxidative aging). This is attributed to the shorter molecular chain of aged PTFE, making it easier to form a molecular film on the surface of the metal friction pairs [71].

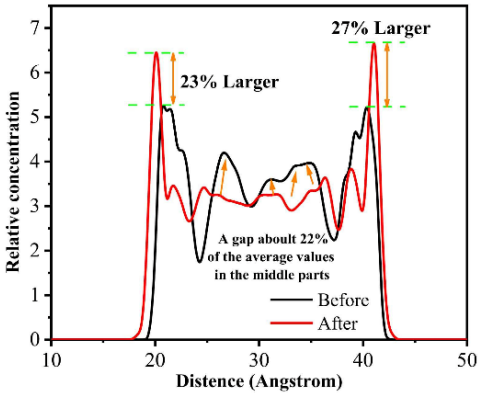


Figure 9. Distribution of the atomic concentration of PTFE in the extended thickness direction during friction, as determined before and after thermal oxidative ageing [71].

3.1.6. Radial Distribution Function (RDF)

RDF can be simply explained as the ratio of the local density to the global density of the system, which is defined as follows:

$$g(r) = \frac{dN}{4\rho\pi r^2 dr} \tag{13}$$

where dN is the number of molecules in the region from r to $r + dr$ away from the central atom, ρ is the global density of the system [72–74]. In polymer tribology, RDF is often used to research the force of the interaction between the components of the friction pairs [75–77]. For instance, Figure 10 illustrates the RDF curves between Cu and C (Cu is the center atom) in Cu/PTFE and Cu/(CNT/PTFE) friction experiments. With the same r value, the former always has a higher g(r) value than the latter, which indicates that Cu has a stronger effect with pure PTFE, i.e., CNT has a strong binding effect on PTFE molecules, which serves the purpose of reducing wear [78].

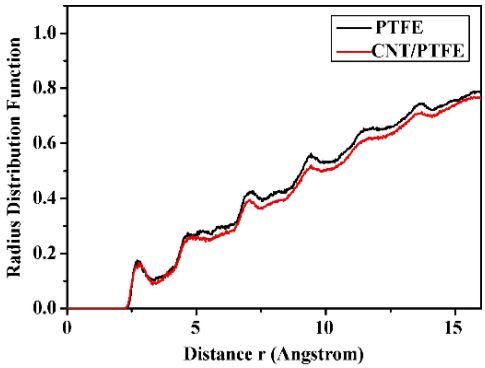


Figure 10. RDF values of the Cu atoms and C atoms of the PTFE and CNTs/PTFE composite during the process of wear [78].

3.1.7. Conformation of Polymers

The friction process is usually accompanied by shearing and extrusion, which causes conformational changes in the polymer chains. This evolution consists of two aspects. One

is the degree of curl of polymer molecules; this is generally described by the radius of gyration R_g. It is defined as follows:

$$R_g^2 = \frac{1}{M}\sum_i m_i(r_i - r_{cm})^2 \quad (14)$$

where M is the total mass of the polymer chain, and r_{cm} is the center-of-mass of the polymer chain [79,80]. The radius of gyration evolution of pure NBR, NBR/SiO_2, and NBR/$SiO_{2(TESPT)}$ during boundary lubrication and dry friction processes was recorded by Liu et al. As shown in Figure 11, the radius of gyration of all polymer chains tends to increase under both boundary lubrication and dry friction conditions, i.e., the chains unfold with a friction effect. Furthermore, the increase of the radius of gyration of NBR molecules in NBR/$SiO_{2(TESPT)}$ is minimal, which is attributed to the strong adsorption of modified SiO_2 on NBR. This indicates that the modified SiO_2 can increase the strength of NBR, thus reducing the wear [81].

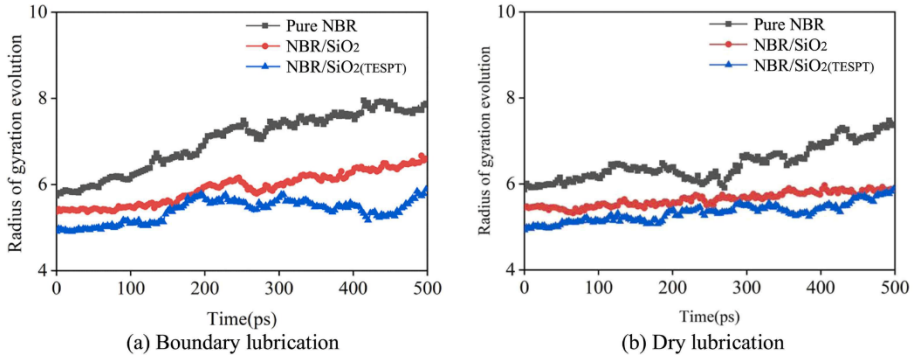


Figure 11. Radius of gyration evolution of NBR molecular chains under different lubrication conditions (friction modeled as a copper bar sliding on a polymer matrix covered with a water layer). (**a**) Boundary lubrication (the copper bar moving down to the interface between the water layer and the polymer). (**b**) Dry lubrication [81].

The other is the resonance variation of bond lengths and bond angles within the polymer molecule. This change helps to understand the interactions between molecular chains. Liu et al. explored conformational changes of perfluoropolyethers (PFPE) as the lubricant under high pressure lubrication conditions (Figure 12). The results demonstrated that at 1.0 GPa, the bond lengths and bond angles changed significantly within the first 0.8 ns, after which they almost reached a steady state [82].

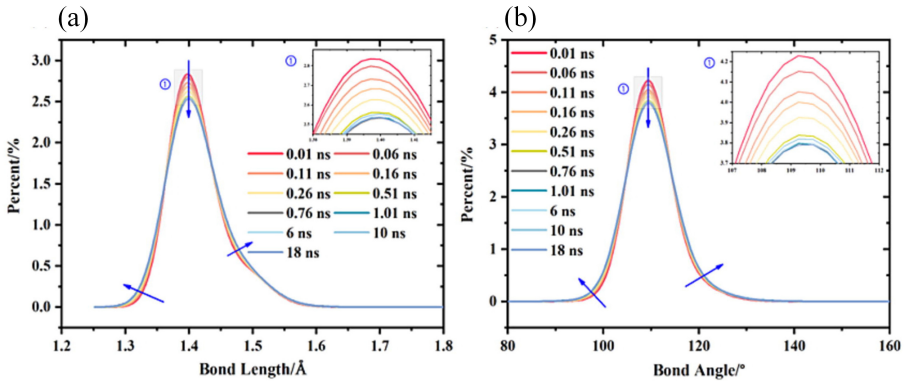


Figure 12. (**a**) Bond length distribution evolution during the simulation under 1.0 GPa. (**b**) Bond angle distribution evolution during the simulation under 1.0 GPa. The friction model is an Fe/PFPE/Fe three-layer structure [82].

3.1.8. Velocity Distribution

Shear not only affects the conformation of polymer molecules but also causes a change in its velocity along the shear direction; exploring this velocity evolution can facilitate understanding of the microscopic friction mechanisms of polymers [82–85]. Figure 13 shows the velocity distribution curves of atoms in the NBR matrix containing different mass fractions of CNT along the z-axis direction. As can be seen from the local magnification of the curves, the more CNT is added to NBR, the smaller the change of its velocity at the interface is, i.e., a reasonable amount of CNT can improve the abrasion resistance of NBR [86].

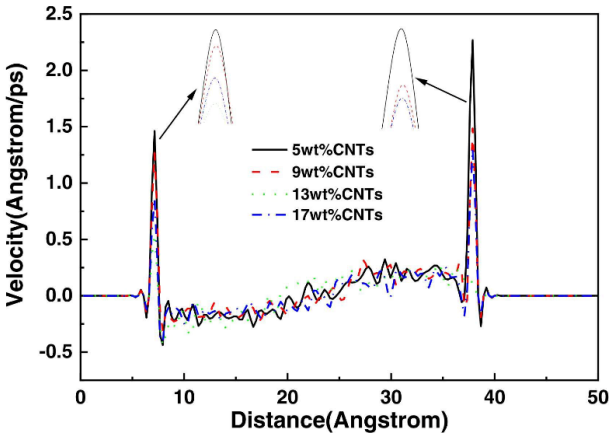


Figure 13. Velocity distribution of CNT/NBR composites [86].

3.1.9. Temperature Variation

Friction typically induces an increase in temperature between the contacting interfaces. This results in localized softening of the polymer material, which weakens its tribological properties [87–89]. Wu et al. investigated the heat generation and temperature distribution at the heterogeneous interface during the Ni/PE friction process. As shown in Figure 14a, PE is susceptible to rapid production of large amounts of heat at the interface due to its large elastic deformation during the friction process. Furthermore, the volume of the area of temperature increase at the PE interface is much larger than that of the metal Ni (Figure 14b), indicating the poor thermal conductivity of PE [90].

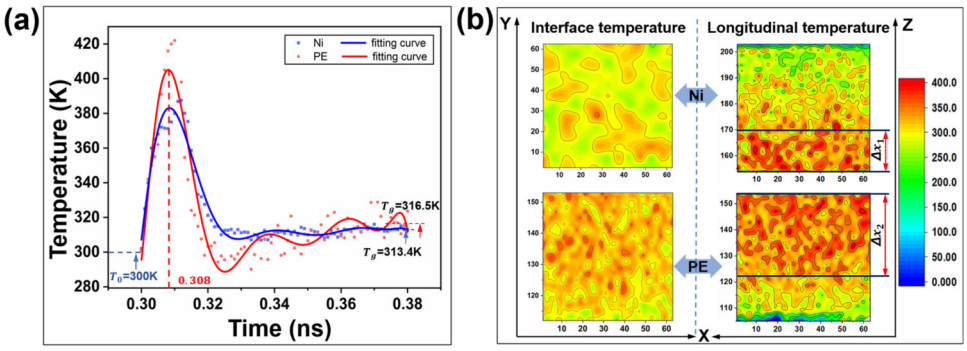


Figure 14. Temperature characteristics at the heterogeneous interface between Ni and PE. (**a**) Variation trend of the average temperature of the PE–Ni interface with time. (**b**) Temperature distribution cloud map of the heterointerface [90].

3.1.10. Energy Analysis

The motion of any object is accompanied by a change in energy, and friction is no exception. Thanks to the richness of the functional form of the all-atom force field, we can not only analyze the variation of potential and kinetic energies in the friction system as a whole, but also study the microscopic friction mechanism of polymers in terms of van der Waals' interaction energy, bonding energy, angular energy, and torsional angular energy [91–93]. As shown in Figure 15, Zhang et al. statistically investigated the energy variation during friction of amorphous PE under different temperature conditions. The variation of angular energy, torsional angular energy, van der Waals interaction energy, and total energy of PE in the glass state is the largest, followed by the transition zone and rubbery state. This indicates that the lower the temperature, the greater the energy change brought about by friction for the PE friction system [94]. Moreover, the enhancement of tribological properties by fillers can also be investigated by analyzing the strength of interaction energy between fillers and polymer matrix; or the friction wear mechanism can be studied based on the strength of interaction between friction pairs [49,95,96].

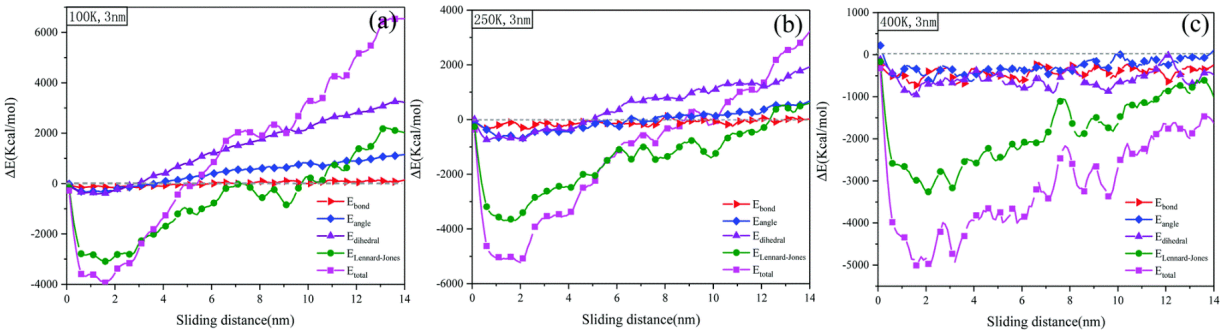


Figure 15. Variation of energy decomposition for amorphous polyethylene in the sliding process for different temperatures: (**a**) 100 K, (**b**) 250 K, and (**c**) 400 K [94].

3.2. Tribochemical Reactions

It has been commonly believed that the investigation of tribochemical reactions is essential for understanding the mechanisms of friction and wear. However, it is difficult to observe in situ the friction chemical reactions between the contact interfaces at the micro/mesoscopic scale due to the current means of characterization [97]. A similar problem exists in the field of polymer tribology [98–100]. Numerous experiments have revealed that a lot of polymers, such as PTFE, PI, and polyether ether ketone (PEEK), also undergo a tribochemical reaction during friction with metals (e.g., Cu and Fe), which is attributed to (1) frictional heat, (2) formation of free radicals due to shear effect, and (3) catalytic effects of metal atoms [97,101–103]. To clarify this evolutionary process, some scholars have introduced the ReaxFF force field, which was originally used to research combustion and catalytic processes, to the analysis of tribochemical reactions. For example, Xu et al. explored the friction chemical reaction process between a single Fe asperity and a PTFE matrix with the introduction of water and oxygen molecules, as depicted in Figure 16a,b. Throughout the friction process, the asperity causes breakage and degradation of the PTFE chains due to pressure and mechanical shear, as illustrated in Figure 16d. This leads to the formation of six different types of friction chemical reaction products, as shown in Figure 16c. Additionally, it is observed from Figure 16e,f that the amounts of Fe-F, Fe-C, and C-O gradually increase with friction [104]. This is remarkable for the understanding of friction and wear mechanisms as well as for the design of novel polymer friction materials.

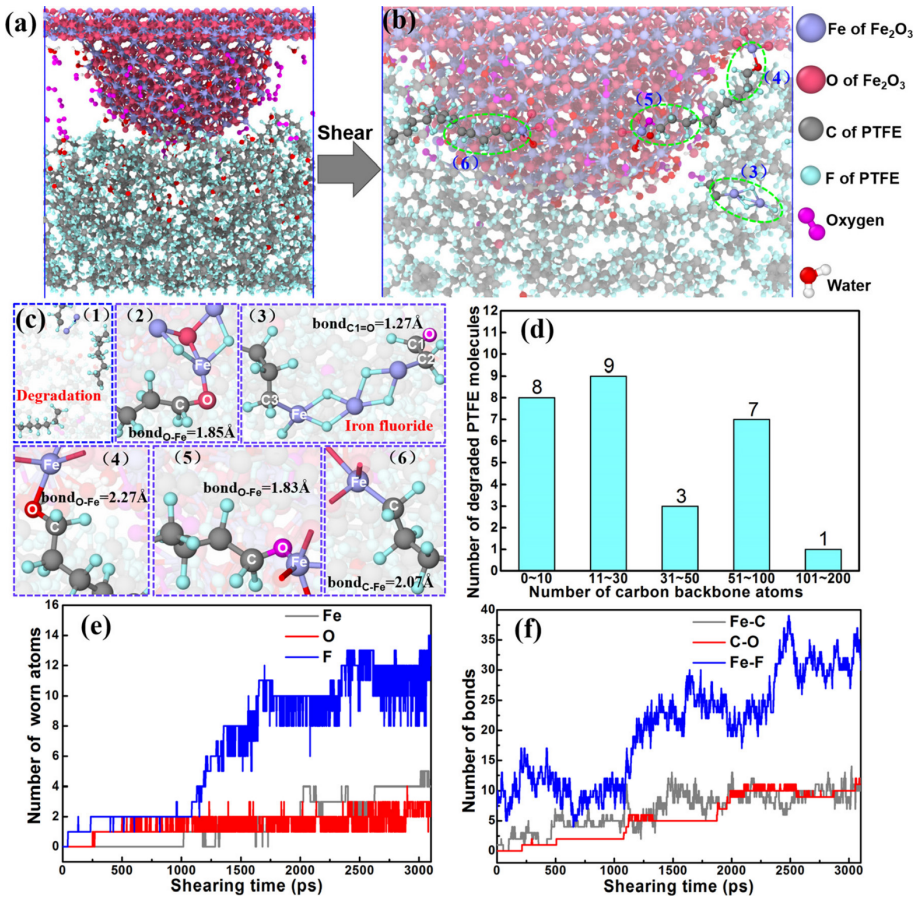


Figure 16. Nanomechanical shear-induced wear and tribochemical reactions in environmental molecules under 4.0 GPa. (**a**) Single asperity under loading conditions. (**b**) Friction shearing induces anchoring chains by tribochemical reactions and bonds. The slice width of a snapshot is 20 Å. (**c**) Tribochemical products and molecular chains anchored by chemical bonds. (**d**) Number of worn and degraded PTFE molecules at a shearing time of 3000 ps. (**e**) Number of worn atoms as a function of shearing time. (**f**) Number of chemical bonds as a function of shearing time [104]. Reprinted (adapted) with permission from [104]. © 2022 American Chemical Society.

3.3. Understanding Friction Process at Larger Spatial and Temporal Scales

MD simulation can usually only simulate the motion of particles at the microscopic scale (i.e., Å or nm for length and fs or ps for time), whereas friction in experiments is a macroscopic behavior; therefore, based on the fact that the data obtained from the two are generally not compatible, it is accurate to say that MD simulation is currently more prone to qualitative analysis [105]. To bridge the gap between MD simulations and actual experiments, several researchers have applied coarse-grained MD simulation to the investigation of polymer tribology. Brownell et al. constructed coarse-grained particles of PTFE with different structures (i.e., porous, flat, and needle) for analyzing their tribological behavior at the micrometer scale (Figure 17). The upper surfaces of these three particles have different peak densities (i.e., number of peaks/upper surface area) and peak heights. As shown in Figure 18, scratching experimental data shows that the PTFE particle with a smooth upper surface (i.e., Figure 17c, the flat one) has the lowest coefficient of friction (~0.03–0.20), which agrees with the experimental data [106]. Furthermore, coarse-grained MD simulation has been applied to study the friction process of polymer brushes, mainly to analyze the forces and collisions of polymer chains and the related friction reduction and lubrication mechanisms [107–111].

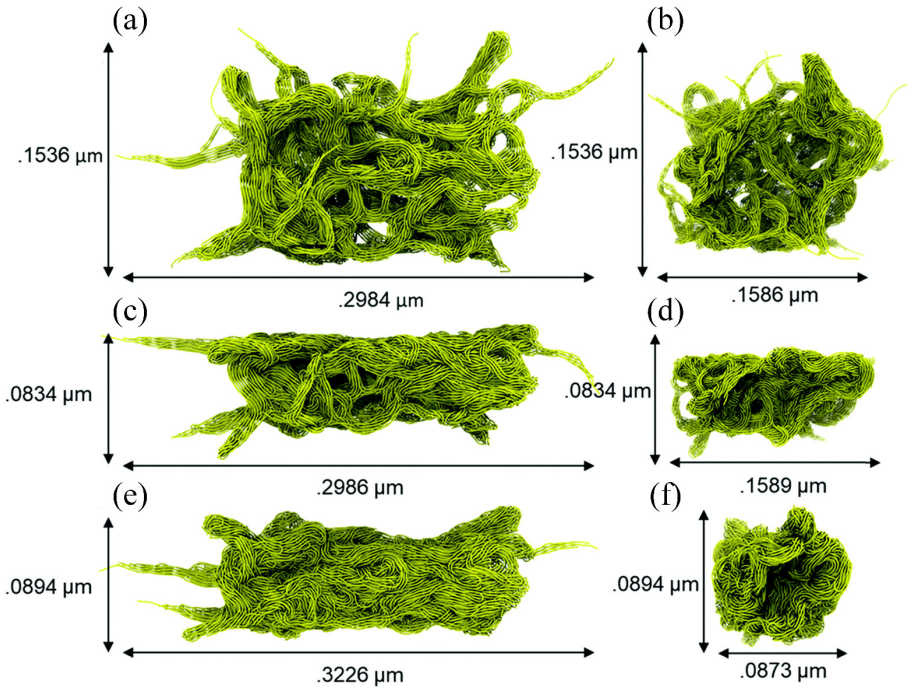


Figure 17. (**a**) A porous particle is generated by equilibrating random PTFE fibers for 15.6 nanoseconds. (**b**) Side view of the porous particle. (**c**) A flattened particle is generated by indenting the porous particle in the Y dimension until the particle is half the original size. (**d**) Side view of the flattened particle. (**e**) A needle particle by varying the density of the PTFE fibers. (**f**) Side view of the needle particle [106].

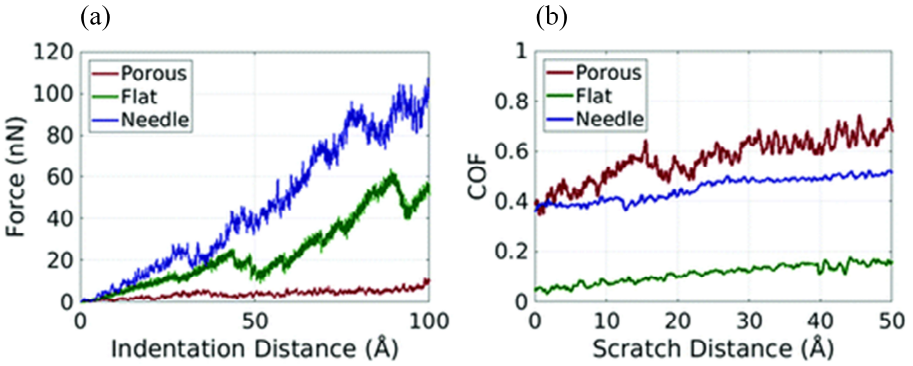


Figure 18. (**a**) Plot of indentation distance vs. indentation force showing that the denser a particle is, the greater the force is needed to indent the same indentation depth. (**b**) Coefficient of friction during the scratch in the X direction [106].

4. Current Challenges in MD Simulation for Polymer Tribology

Recently, MD simulation has attracted much attention as an emerging tool and has gradually developed into one of the indispensable characterization methods in scientific research. Through simulations, we can explore many physicochemical change processes that are currently unobservable by experiments. However, limited by the current state of the technology, MD simulation still has several unsolvable problems. In the following section, a brief overview of these problems is summarized.

4.1. Broadening the Applicability of Force Fields

In MD simulation, for polymers only, the currently developed force fields (e.g., COMPASS, CVFF, PCFF, and OPLS) have almost met expectations in terms of applicability and accuracy. Nevertheless, in practical applications, polymers are usually used as friction

pairs in the form of composite materials (i.e., organic phase/carbon materials or inorganic phase), and the friction pair cooperating with the polymer is usually metal (i.e., composite material/metal phase). At this point, the accuracy of friction simulations based on all-atom force field construction is yet to be proven. Specifically, in the friction simulations of polymer composites constructed on the basis of COMPASS, e.g., NBR/SiO_2, two points need to be pointed out: (1) based on bonding connections, non-bonding interactions are not sufficient to accurately characterize SiO_2 (inorganic phase) particles, and in fact crystalline materials are more accurately described by other force fields, e.g., Tersoff [112]; (2) in the relationship between the NBR and SiO_2 and between metal friction pairs and polymer composites, only van der Waals interactions are simply considered. These have an impact on the accurate description of friction processes in MD simulation.

Starting from the construction of the force field, the ReaxFF force field can be a good solution to the above problem. However, a lot of friction systems may not be constructed due to the current imperfection of the parameter library of this force field. Therefore, it is necessary to broaden the applicability of the related force field to simulate friction systems more accurately in various systems.

4.2. Promoting the Application of Coarse-Grained MD Simulation in Polymer Composites

Coarse-grained MD simulation is of great value as a computational method to reveal the structure and properties of polymer composites at mesoscopic scales. However, from the literature survey, the work based on coarse-grained MD simulation has mainly focused on polymer brushes and pure polymer materials, and very few have covered the tribological properties of polymer composites. On the contrary, there are many works based on all-atom MD simulation involving polymer composites; in these works, the filler additions are often very low (quantities are generally within 5) due to the limitation of the simulation scale, which is not reasonable enough for scientific research. The excellent tribological properties of polymer composites usually cannot be separated from the synergistic effects among their multiple fillers. Hence, there is a necessity to investigate the frictional wear mechanism of polymer matrices containing substantial filler quantities using coarse-grained MD simulation.

5. Conclusions

In summary, MD simulation plays an important role in the study of polymer tribology. It was possible to delve deeply into the analysis of friction and wear mechanisms of polymer/polymer composites at the micro/meso-scale using three mainstream MD research methods, thus transcending the confines of traditional experimental characterization. Especially, MD simulation has further contributed to the understanding of friction processes in three areas: the study of contact interface interaction conditions, energy changes, and tribochemical reactions. Although MD simulation is not yet able to perfectly represent the friction of polymer/polymer composites, such as the absence of a universal force field and limitations in simulating composites at mesoscopic scales. It is believed that with the continuous improvement of technology, such as the introduction of machine learning, enhanced computility, and refinement of MD simulation software, MD simulation results are closer to macro experimental results or providing greater assistance for friction mechanism understanding, advanced polymer design, friction couple selection, and others.

Author Contributions: Writing—original draft preparation, T.Y., Z.G. and Y.P.; writing—review and editing, G.W., J.S. and Q.D.; supervision, G.Z. All authors have read and agreed to the published version of the manuscript.

Funding: This research was funded by the NSFC (52075247, U2037603), Natural Science Foundation of Jiangsu Province (BK20210300), a project funded by the Priority Academic Program Development of Jiangsu Higher Education Institutions (PAPD).

Data Availability Statement: No new data were created or analyzed in this study. Data sharing is not applicable to this article.

Conflicts of Interest: The authors declare no conflicts of interest.

References

1. Yadav, R.; Singh, M.; Shekhawat, D.; Lee, S.-Y.; Park, S.-J. The role of fillers to enhance the mechanical, thermal, and wear characteristics of polymer composite materials: A review. *Compos. Part A Appl. Sci. Manuf.* **2023**, *175*, 107775. [CrossRef]
2. Kurdi, A.; Chang, L. Recent advances in high performance polymers—Tribological aspects. *Lubricants* **2018**, *7*, 2. [CrossRef]
3. Myshkin, N.; Kovalev, A. Adhesion and surface forces in polymer tribology—A review. *Friction* **2018**, *6*, 143–155. [CrossRef]
4. Chan, J.X.; Wong, J.F.; Petru, M.; Hassan, A.; Nirmal, U.; Othman, N.; Ilyas, R.A. Effect of nanofillers on tribological properties of polymer nanocomposites: A review on recent development. *Polymers* **2021**, *13*, 2867. [CrossRef]
5. Mohammed, L.; Ansari, M.N.M.; Pua, G.; Jawaid, M.; Islam, M.S. A review on natural fiber reinforced polymer composite and its applications. *Int. J. Polym. Sci.* **2015**, *2015*, 243947. [CrossRef]
6. Srivastava, I.; Kotia, A.; Ghosh, S.K.; Ali, M.K.A. Recent advances of molecular dynamics simulations in nanotribology. *J. Mol. Liq.* **2021**, *335*, 116154. [CrossRef]
7. Rossetti, G.; Mandelli, D. How exascale computing can shape drug design: A perspective from multiscale QM/MM molecular dynamics simulations and machine learning-aided enhanced sampling algorithms. *Curr. Opin. Struct. Biol.* **2024**, *86*, 102814. [CrossRef]
8. Bera, I.; Payghan, P.V. Use of molecular dynamics simulations in structure-based drug discovery. *Curr. Pharm. Des.* **2019**, *25*, 3339–3349. [CrossRef]
9. Jónsson, E. Ionic liquids as electrolytes for energy storage applications—A modelling perspective. *Energy Storage Mater.* **2020**, *25*, 827–835. [CrossRef]
10. Formalik, F.; Shi, K.; Joodaki, F.; Wang, X.; Snurr, R.Q. Exploring the structural, dynamic, and functional properties of metal-organic frameworks through molecular modeling. *Adv. Funct. Mater.* **2023**, 2308130. [CrossRef]
11. Zhou, W.; Wei, M.; Zhang, X.; Xu, F.; Wang, Y. Fast desalination by multilayered covalent organic framework (COF) nanosheets. *ACS Appl. Mater. Interfaces* **2019**, *11*, 16847–16854. [CrossRef] [PubMed]
12. Ewen, J.P.; Heyes, D.M.; Dini, D. Advances in nonequilibrium molecular dynamics simulations of lubricants and additives. *Friction* **2018**, *6*, 349–386. [CrossRef]
13. Talapatra, A.; Datta, D. A review of the mechanical, thermal and tribological properties of graphene reinforced polymer nanocomposites: A molecular dynamics simulations methods. *Polym. Bull.* **2022**, *80*, 2299–2328. [CrossRef]
14. Kmiecik, S.; Gront, D.; Kolinski, M.; Wieteska, L.; Dawid, A.E.; Kolinski, A. Coarse-grained protein models and their applications. *Chem. Rev.* **2016**, *116*, 7898–7936. [CrossRef] [PubMed]
15. Sun, H. COMPASS: An ab initio force-field optimized for condensed-phase applicationss-overview with details on alkane and benzene compounds. *J. Phys. Chem. B* **1998**, *102*, 7338–7364. [CrossRef]
16. Sun, H.; Jin, Z.; Yang, C.; Akkermans, R.L.; Robertson, S.H.; Spenley, N.A.; Miller, S.; Todd, S.M. COMPASS II: Extended coverage for polymer and drug-like molecule databases. *J. Mol. Model* **2016**, *22*, 47. [CrossRef] [PubMed]
17. Akkermans, R.L.C.; Spenley, N.A.; Robertson, S.H. COMPASS III: Automated fitting workflows and extension to ionic liquids. *Mol. Simul.* **2020**, *47*, 540–551. [CrossRef]
18. Dauber-Osguthorpe, P.; Roberts, V.A.; Osguthorpe, D.J.; Wolff, J.; Genest, M.; Hagler, A.T. Structure and energetics of ligand binding to proteins: Escherichia coli dihydrofolate reductase-trimethoprim, a drug-receptor system. *Proc. Nati. Acad. Sci. USA* **1988**, *4*, 31–47.
19. Maple, J.R.; Dinur, U.; Hagler, A.T. Derivation of force fields for molecular mechanics and dynamics from ab initio energy surfaces. *Proc. Nati. Acad. Sci. USA* **1988**, *85*, 5350–5354. [CrossRef]
20. Gaedt, K.; Hltje, H.-D. Consistent valence force-field parameterization of bond lengths and angles with quantum chemicalab initio methods applied to some heterocyclic dopamine D3-receptor agonists. *J. Comput. Chem.* **1998**, *19*, 935–946. [CrossRef]
21. Lange, J.; de Souza, F.G.; Nele, M.; Tavares, F.W.; Segtovich, I.S.V.; da Silva, G.C.Q.; Pinto, J.C. Molecular dynamic simulation of oxaliplatin diffusion in poly(lactic acid-co-glycolic acid). Part a: Parameterization and validation of the force-field CVFF. *Macromol. Theory Simul.* **2016**, *25*, 45–62. [CrossRef]
22. Sun, H.; Mumby, S.J.; Maple, J.R.; Hagler, A.T. An ab Initio CFF93 All-Atom Force Field for Polycarbonates. *J. Am. Chem. Soc.* **1994**, *116*, 2978–2987. [CrossRef]
23. Sun, H. Ab Initio Calculations and Force Field Development for Computer Simulation of Polysilanes. *Macromolecules* **1995**, *28*, 701–712. [CrossRef]
24. Jorgensen, W.L.; Maxwell, D.S.; Tirado-Rives, J. Development and testing of the OPLS all-atom force field on conformational energetics and properties of organic liquids. *J. Am. Chem. Soc.* **1996**, *118*, 11225–11236. [CrossRef]
25. Doherty, B.; Zhong, X.; Gathiaka, S.; Li, B.; Acevedo, O. Revisiting OPLS force field parameters for ionic liquid simulations. *J. Chem. Theory Comput.* **2017**, *13*, 6131–6145. [CrossRef] [PubMed]
26. Robertson, M.J.; Tirado-Rives, J.; Jorgensen, W.L. Improved peptide and protein torsional energetics with the OPLS-AA force field. *J. Chem. Theory Comput.* **2015**, *11*, 3499–3509. [CrossRef] [PubMed]
27. Kaminski, G.A.; Friesner, R.A.; Tirado-Rives, J.; Jorgensen, W.L. Evaluation and reparametrization of the OPLS-AA force field for proteins via comparison with accurate quantum chemical calculations on peptides. *J. Phys. Chem. B* **2001**, *105*, 6474–6487. [CrossRef]

28. Van Duin, A.C.T.; Dasgupta, S.; Lorant, F.; Goddard, W.A. ReaxFF: A reactive force field for hydrocarbons. *J. Phys. Chem. A* **2001**, *105*, 9396–9409. [CrossRef]
29. Senftle, T.P.; Hong, S.; Islam, M.M.; Kylasa, S.B.; Zheng, Y.; Shin, Y.K.; Junkermeier, C.; Engel-Herbert, R.; Janik, M.J.; Aktulga, H.M.; et al. The ReaxFF reactive force-field: Development, applications and future directions. *npj Comput. Mater.* **2016**, *2*, 15011. [CrossRef]
30. Russo, M.F.; van Duin, A.C.T. Atomistic-scale simulations of chemical reactions: Bridging from quantum chemistry to engineering. *Nucl. Instrum. Methods Phys. Res.* **2011**, *269*, 1549–1554. [CrossRef]
31. van Duin, A.C.T.; Strachan, A.; Stewman, S.; Zhang, Q.; Xu, X.; Goddard, W.A. ReaxFFSiO reactive force field for silicon and silicon oxide systems. *J. Phys. Chem. A* **2003**, *107*, 3803–3811. [CrossRef]
32. Karimi-Varzaneh, H.A.; van der Vegt, N.F.A.; Müller-Plathe, F.; Carbone, P. How good are coarse-grained polymer models? A comparison for atactic polystyrene. *ChemPhysChem* **2012**, *13*, 3428–3439. [CrossRef] [PubMed]
33. Singh, N.; Li, W. Recent advances in coarse-grained models for biomolecules and their applications. *Int. J. Mol. Sci.* **2019**, *20*, 3774. [CrossRef] [PubMed]
34. Saunders, M.G.; Voth, G.A. Coarse-graining methods for computational biology. *Annu. Rev. Biophys.* **2013**, *42*, 73–93. [CrossRef] [PubMed]
35. Gao, H.; Shi, R.; Zhu, Y.; Qian, H.; Lu, Z. Coarse-grained dynamics simulation in polymer systems: From structures to material properties. *Chem. Res. Chin. Univ.* **2022**, *38*, 653–670. [CrossRef]
36. Souza, P.C.T.; Alessandri, R.; Barnoud, J.; Thallmair, S.; Faustino, I.; Grünewald, F.; Patmanidis, I.; Abdizadeh, H.; Bruininks, B.M.H.; Wassenaar, T.A.; et al. Martini 3: A general purpose force field for coarse-grained molecular dynamics. *Nat. Methods* **2021**, *18*, 382–388. [CrossRef]
37. Weiand, E.; Koenig, P.H.; Rodriguez-Ropero, F.; Roiter, Y.; Angioletti-Uberti, S.; Dini, D.; Ewen, J.P. Boundary lubrication performance of polyelectrolyte-surfactant complexes on biomimetic surfaces. *Langmuir* **2024**, *40*, 7933–7946. [CrossRef] [PubMed]
38. Adroher-Benítez, I.; Morozova, T.I.; Catalini, G.; García, N.A.; Barrat, J.-L.; Luengo, G.S.; Léonforte, F. Effect of polymer architecture on the adsorption and coating stability on heterogeneous biomimetic surfaces. *Macromolecules* **2023**, *56*, 10285–10295. [CrossRef]
39. Coscia, B.J.; Shelley, J.C.; Browning, A.R.; Sanders, J.M.; Chaudret, R.; Rozot, R.; Leonforte, F.; Halls, M.D.; Luengo, G.S. Shearing friction behaviour of synthetic polymers compared to a functionalized polysaccharide on biomimetic surfaces: Models for the prediction of performance of eco-designed formulations. *Phys. Chem. Chem. Phys.* **2023**, *25*, 1768–1780. [CrossRef]
40. Yin, Y.; Song, J.; Zhao, G.; Ding, Q. Improving the high temperature tribology of polyimide by molecular structure design and grafting POSS. *Polym. Adv. Technol.* **2021**, *33*, 886–896. [CrossRef]
41. Liu, C.; Song, J.; Zhao, G.; Yin, Y.; Ding, Q. Improving thermal conductivity and tribological performance of polyimide by filling Cu, CNT, and graphene. *Micromachines* **2023**, *14*, 616. [CrossRef] [PubMed]
42. Qian, C.; Li, Y.; Zhao, J.; Wang, S.; He, E. Thermal-oxidative aging and tribological properties of carbon nanotube/nitrile butadiene rubber composites with varying acrylonitrile content: Molecular dynamics simulations. *Polym Eng Sci.* **2023**, *63*, 1516–1527. [CrossRef]
43. Wu, J.; Teng, F.; Su, B.; Wang, Y. Molecular dynamics study on tribological properties of EUG/NR composites. *Comput. Mater. Sci.* **2021**, *199*, 110732. [CrossRef]
44. Li, X.; Li, Y.; Qian, C.; Zhao, J.; Wang, S. Molecular dynamics study of the mechanical and tribological properties of graphene oxide-reinforced polyamide 66/nitrile butadiene rubber composites. *Appl. Phys. A* **2023**, *129*, 276. [CrossRef]
45. Cai, P.; Xu, C.; Zheng, F.; Song, J.; Zhao, G. Molecular dynamics study on the mechanical and tribological properties of polyimide reinforced by lanthana. *Ind. Lubr. Tribol.* **2021**, *73*, 1319–1324. [CrossRef]
46. Cui, J.; Zhao, J.; Wang, S.; Wang, Y.; Li, Y. Effects of carbon nanotubes functionalization on mechanical and tribological properties of nitrile rubber nanocomposites: Molecular dynamics simulations. *Comput. Mater. Sci.* **2021**, *196*, 110556. [CrossRef]
47. Yuan, Q.; Li, Y.; Wang, S.; He, E.; Yang, B.; Nie, R. A Molecular Dynamics Simulation Study on Enhancement of Mechanical and Tribological Properties of Nitrile-Butadiene Rubber with Varied Contents of Acrylonitrile. *Polymers* **2023**, *15*, 3799. [CrossRef]
48. Li, S.; Dong, C.; Yuan, C.; Bai, X. Molecular dynamics simulation on performance modulation of graphene-modified polyethylene during friction process. *Polym. Adv. Technol.* **2022**, *33*, 3479–3489. [CrossRef]
49. Cui, J.; Zhao, J.; Wang, S.; Li, Y. A comparative study on enhancement of mechanical and tribological properties of nitrile rubber composites reinforced by different functionalized graphene sheets: Molecular dynamics simulations. *Polym. Compos.* **2020**, *42*, 205–219. [CrossRef]
50. Qian, C.; Li, Y.; Zhao, J.; Wang, S. Effect of single-vacancy- and vacancy-adsorbed-atom-defective CNTs on the mechanical and tribological properties of NBR composites: Molecular dynamics simulations. *J. Polym. Res.* **2023**, *30*, 99. [CrossRef]
51. Wang, M.; Li, Y.; Qian, C.; Zhao, J.; Wang, S. Molecular dynamics simulations of defective carbon nanotubes on the aging and friction properties of nitrile butadiene rubber composites. *Polym. Compos.* **2022**, *44*, 1228–1239. [CrossRef]
52. Yang, Z.; Guo, Z.; Yuan, C.; Bai, X. Tribological behaviors of composites reinforced by different functionalized carbon nanotube using molecular dynamic simulation. *Wear* **2021**, *476*, 203669. [CrossRef]
53. Zuo, Z.; Liang, L.; Bao, Q.; Yan, P.; Jin, X.; Yang, Y. Molecular dynamics calculation on the adhesive interaction between the polytetrafluoroethylene transfer film and iron surface. *Front. Chem.* **2021**, *9*, 740447. [CrossRef] [PubMed]

54. Stukowski, A. Visualization and analysis of atomistic simulation data with OVITO–the Open Visualization Tool. *Model. Simul. Mater. Sci. Eng.* **2010**, *18*, 015012. [CrossRef]
55. Humphrey, W.; Dalke, A.; Schulten, K. VMD: Visual Molecular Dynamics. *J. Mol. Graph.* **1996**, *14*, 33–38. [CrossRef] [PubMed]
56. Wang, R.; Huang, H.; Qu, J.; Ren, R.; He, H.; Huang, F.; Wang, Y. Frictional anisotropy of oriented carbon nanotubes/rubber composites and new insight into its mechanism from the perspective of frictional interface. *J. Tribol.* **2023**, *145*, 011704. [CrossRef]
57. Li, Y.; Wang, S.; Arash, B.; Wang, Q. A study on tribology of nitrile-butadiene rubber composites by incorporation of carbon nanotubes: Molecular dynamics simulations. *Carbon* **2016**, *100*, 145–150. [CrossRef]
58. Teng, F.; Wu, J.; Su, B.; Wang, Y. Enhanced adhesion friction behaviors of nature rubber composites by applications of carbon nanotube: Experiment and molecular insight. *Tribol. Int.* **2023**, *181*, 108333. [CrossRef]
59. Li, C.; Huang, H.; Qu, J.; Cao, J.; Huang, F.; Wang, Y. Mechanism of wear and COF variation of vulcanized rubber under changing loads and sliding velocities: Interpretation at the atomic scale. *Tribol. Int.* **2022**, *170*, 107505. [CrossRef]
60. Yin, B.B.; Huang, J.S.; Ji, W.M.; Liew, K.M. Exploring frictional performance of diamond nanothread reinforced polymer composites from the atomistic simulation and density functional theory. *Carbon* **2022**, *200*, 10–20. [CrossRef]
61. Wei, Q.; Wang, Y.; Rao, Y.; Jiang, A.; Zhang, K.; Lu, T.; Chen, X. Evaluating the effects of nanosilica on mechanical and tribological properties of polyvinyl alcohol/polyacrylamide polymer composites for artificial cartilage from an atomic level. *Polymers* **2019**, *11*, 76. [CrossRef] [PubMed]
62. Song, J.; Zhao, G. A molecular dynamics study on water lubrication of PTFE sliding against copper. *Tribol. Int.* **2019**, *136*, 234–239. [CrossRef]
63. Wang, W.; Zhang, X.; Li, Y.; Huang, R.; Xu, J.; Yang, L. Effects of molecular structures of poly α-olefin mixture on nano-scale thin film lubrication. *Mater. Today Commun.* **2020**, *25*, 101500. [CrossRef]
64. Yang, Y.; Zhao, J.; Cui, J.; Jiang, B. Molecular dynamics study on enhancement of mechanical and tribological properties of polytetrafluoroethylene composites by incorporating hexagonal boron nitride nanosheets. *J. Appl. Polym. Sci.* **2023**, *140*, e53761. [CrossRef]
65. Zheng, T.; Wang, S.; Zhou, L.; Li, X.; Zhang, H. The disentanglement and shear properties of amorphous polyethylene during friction: Insights from molecular dynamics simulations. *Appl. Surf. Sci.* **2022**, *580*, 152301. [CrossRef]
66. Vacher, R.; de Wijn, A.S. Nanoscale friction and wear of a polymer coated with graphene. *Beilstein J. Nanotechnol.* **2022**, *13*, 63–73. [CrossRef] [PubMed]
67. Qi, Y.; Sun, B.; Zhang, Y.; Gao, G.; Zhang, P.; Zheng, X. Tribological Properties of Nano-ZrO_2 and PEEK Reinforced PTFE Composites Based on Molecular Dynamics. *Lubricants* **2023**, *11*, 194. [CrossRef]
68. Xu, M.; Wang, T.; Wang, Q.; Zhang, X.; Tao, L.; Li, S. Mechanical and tribological properties of polytetrafluoroethylene reinforced by nano-ZrO2: Molecular dynamic simulation. *High Perform. Polym.* **2022**, *34*, 397–405. [CrossRef]
69. Teng, F.; Wu, J.; Su, B.; Wang, Y. Enhanced tribological properties of vulcanized natural rubber composites by applications of carbon nanotube: A molecular dynamics study. *Nanomaterials* **2021**, *11*, 2646. [CrossRef]
70. Chawla, R.; Sharma, S. A molecular dynamics study on Young's modulus and tribology of carbon nanotube reinforced styrene-butadiene rubber. *J. Mol. Model.* **2018**, *24*, 96. [CrossRef]
71. Qu, F.; Liu, L.; Tao, G.; Zhan, W.; Zhan, S.; Li, Y.; Li, C.; Lv, X.; Shi, Z.; Duan, H. Effect of thermal oxidative ageing on the molecular structure and tribological properties of polytetrafluoroethylene. *Tribol. Int.* **2023**, *188*, 108850. [CrossRef]
72. Zhang, T.; Huang, H.; Li, W.; Chang, X.; Cao, J.; Hua, L. Vulcanization vodeling and mechanism for improved tribological performance of styrene-butadiene rubber at the atomic scale. *Tribol. Lett.* **2020**, *68*, 83. [CrossRef]
73. Xu, Q.; Zhang, J.; Hu, Y.-Z.; Ma, T.-B. Tribological rehavior of poly(tetrafluoroethylene) and Its composites reinforced by carbon nanotubes and graphene sheets: Molecular dynamics simulation. *Phys. Status Solidi RRL* **2021**, *16*, 2100298. [CrossRef]
74. Wang, Z.; Su, M.; Duan, X.; Yao, X.; Han, X.; Song, J.; Ma, L. Molecular dynamics simulation of the thermomechanical and tribological properties of graphene-reinforced natural rubber nanocomposites. *Polymers* **2022**, *14*, 5056. [CrossRef] [PubMed]
75. Li, Y.; Wang, S.; He, E.; Wang, Q. The effect of sliding velocity on the tribological properties of polymer/carbon nanotube composites. *Carbon* **2016**, *106*, 106–109. [CrossRef]
76. Xu, M.; Wang, Q.; Wang, T.; Tao, L.; Li, S. Molecular dynamic simulation study of tribological mechanism of PI composites reinforced by CNTs with different orientations. *Polym. Compos.* **2022**, *43*, 1557–1565. [CrossRef]
77. Sun, W.; Ye, J.; Liu, X.; Liu, K. Atomistic insights into anti-wear mechanisms and protective tribofilm formation in polytetrafluoroethylene composites. *J. Tribol.* **2022**, *144*, 091701. [CrossRef]
78. Song, J.; Lei, H.; Zhao, G. Improved mechanical and tribological properties of polytetrafluoroethylene reinforced by carbon nanotubes: A molecular dynamics study. *Comput. Mater. Sci.* **2019**, *168*, 131–136. [CrossRef]
79. Liu, X.; Zhou, X.; Kuang, F.; Zuo, H.; Huang, J. Mechanical and tribological properties of nitrile rubber reinforced by nano-SiO2: Molecular dynamics simulation. *Tribol. Lett.* **2021**, *69*, 54. [CrossRef]
80. Song, J.; Zhao, G.; Ding, Q.; Yang, Y. Molecular dynamics study on the thermal, mechanical and tribological properties of PBI/PI composites. *Mater. Today Commun.* **2022**, *30*, 103077. [CrossRef]
81. Liu, X.; Huang, J.; Yang, C.; Xing, S.; Wang, P.; Zhou, X. Molecular dynamics simulations probing the effects of interfacial interactions on the tribological properties of nitrile butadiene rubber/nano-SiO_2 under water lubrication. *Mater. Today Commun.* **2022**, *32*, 104165. [CrossRef]

82. Liu, D.; Li, H.; Huo, L.; Wang, K.; Sun, K.; Wei, J.; Chen, F. Molecular dynamics simulation of the lubricant conformation changes and energy transfer of the confined thin lubricant film. *Chem. Eng. Sci.* **2023**, *270*, 118541. [CrossRef]
83. He, E.; Wang, S.; Tang, L.; Chen, J. A study on the enhancement of the tribological properties of nitrile-butadiene rubber reinforced by nano-ZnO particles from an atomic view. *Mater. Res. Express* **2021**, *8*, 095009. [CrossRef]
84. von Goeldel, S.; Reichenbach, T.; König, F.; Mayrhofer, L.; Moras, G.; Jacobs, G.; Moseler, M. A combined experimental and atomistic investigation of PTFE double transfer film formation and lubrication in rolling point contacts. *Tribol. Lett.* **2021**, *69*, 136. [CrossRef]
85. Cheng, G.; Chen, B.; Guo, F.; Xiang, C.; Jia, X. Research on the friction and wear mechanism of a polymer interface at low temperature based on molecular dynamics simulation. *Tribol. Int.* **2023**, *183*, 108396. [CrossRef]
86. Li, C.; Liu, Z.; Huo, Y.; Li, F.; Tang, L. Molecular dynamics simulation of mechanical and tribological properties of nitrile butadiene rubber with different length and content carbon nanotubes. *Mater. Today Commun.* **2023**, *36*, 106693. [CrossRef]
87. Xu, M.; Wang, X.; Wang, T.; Wang, Q.; Li, S. Ag nanoparticle decorated graphene for improving tribological properties of fabric/phenolic composites. *Tribol. Int.* **2022**, *176*, 107889. [CrossRef]
88. Qiang, Y.; Wu, W.; Lu, J.; Jiang, B.; Ziegmann, G. Progressive molecular rearrangement and heat generation of amorphous polyethene under sliding friction: Insight from the united-atom molecular dynamics simulations. *Langmuir* **2020**, *36*, 11303–11315. [CrossRef] [PubMed]
89. Peng, Y.; Li, J.; Tang, X.; Yang, W.; Chen, X.; Fan, C.; Wang, K. Molecular dynamics study on the tribological properties of phosphorene/polyethylene composites. *Coatings* **2019**, *9*, 342. [CrossRef]
90. Wu, W.; He, C.; Qiang, Y.; Peng, H.; Zhou, M. Polymer-metal interfacial friction characteristics under ultrasonic plasticizing conditions: A united-atom molecular dynamics study. *Int. J. Mol. Sci.* **2022**, *23*, 2829. [CrossRef]
91. Yang, Y.; Zhao, J.; Cui, J.; Jiang, B. Enhanced mechanical and tribological properties of polymer nanocomposites by improving interfacial properties by hexagonal boron nitride nanosheets: Molecular dynamics simulations. *J. Appl. Polym. Sci.* **2023**, *140*, e54340. [CrossRef]
92. Hu, C.; Qi, H.; Song, J.; Zhao, G.; Yu, J.; Zhang, Y.; He, H.; Lai, J. Exploration on the tribological mechanisms of polyimide with different molecular structures in different temperatures. *Appl. Surf. Sci.* **2021**, *560*, 150051. [CrossRef]
93. Li, Y.; Wang, S.; Wang, Q.; Xing, M. Molecular dynamics simulations of tribology properties of NBR (Nitrile-Butadiene Rubber) /carbon nanotube composites. *Compos. Part B Eng.* **2016**, *97*, 62–67. [CrossRef]
94. Zhan, S.; Xu, H.; Duan, H.; Pan, L.; Jia, D.; Tu, J.; Liu, L.; Li, J. Molecular dynamics simulation of microscopic friction mechanisms of amorphous polyethylene. *Soft Matter* **2019**, *15*, 8827–8839. [CrossRef] [PubMed]
95. He, E.; Wang, S.; Li, Y.; Wang, Q. Enhanced tribological properties of polymer composites by incorporation of nano-SiO_2 particles: A molecular dynamics simulation study. *Comput. Mater. Sci.* **2017**, *134*, 93–99. [CrossRef]
96. Li, Y.; Wang, S.; Wang, Q. Enhancement of tribological properties of polymer composites reinforced by functionalized graphene. *Compos. Part B Eng.* **2017**, *120*, 83–91. [CrossRef]
97. Chen, Y.; Renner, P.; Liang, H. A review of current understanding in tribochemical reactions involving lubricant additives. *Friction* **2022**, *11*, 489–512. [CrossRef]
98. Xu, Q.; Tang, X.; Zhang, J.; Hu, Y.; Ma, T. Unraveling tribochemistry and self-Lubrication mechanism of polytetrafluoroethylene by reactive coarse-grained molecular dynamics simulations. *ACS Appl. Mater. Interfaces* **2023**, *15*, 45506–45515. [CrossRef] [PubMed]
99. Katsukawa, R.; Van Sang, L.; Tomiyama, E.; Washizu, H. High-Pressure Lubrication of Polyethylethylene by Molecular Dynamics Approach. *Tribol. Lett.* **2022**, *70*, 101. [CrossRef]
100. Zheng, T.; Gu, J.; Zhang, Y.; Zhang, H. Evolution of the microstructure of amorphous polyethylene under friction-induced plastic flows: A reactive molecular investigation. *J. Chem. Phys.* **2023**, *159*, 104309. [CrossRef]
101. Onodera, T.; Kawasaki, K.; Nakakawaji, T.; Higuchi, Y.; Ozawa, N.; Kurihara, K.; Kubo, M. Tribocatalytic Reaction of Polytetrafluoroethylene Sliding on an Aluminum Surface. *J. Phys. Chem. C* **2015**, *119*, 15954–15962. [CrossRef]
102. Zheng, F.; Lv, M.; Wang, Q.; Wang, T. Effect of temperature on friction and wear behaviors of polyimide (PI)-based solid-liquid lubricating materials. *Polym. Adv. Technol.* **2015**, *26*, 988–993. [CrossRef]
103. Zhou, X.; Zhang, Y.; Guo, P.; Cui, L.; Wang, A.; Ke, P. Tribological behavior of Cr/a-C multilayered coating against PEEK under dry sliding condition. *Wear* **2023**, *518–519*, 204625. [CrossRef]
104. Xu, Q.; Zhang, J.; Li, X.; van Duin, D.M.; Hu, Y.; van Duin, A.C.T.; Ma, T. How polytetrafluoroethylene lubricates iron: An atomistic view by reactive molecular dynamics. *ACS Appl. Mater. Interfaces* **2022**, *14*, 6239–6250. [CrossRef] [PubMed]
105. Pan, D.; Wang, H.; Sun, L.; Zhu, K.; Hao, X. Effect of temperature on Fe–polytetrafluoroethylene friction coefficient using molecular dynamics simulation. *Tribol. Trans.* **2022**, *65*, 705–715. [CrossRef]
106. Brownell, M.; Nair, A.K. Deformation mechanisms of polytetrafluoroethylene at the nano- and microscales. *Phys. Chem. Chem. Phys.* **2018**, *21*, 490–503. [CrossRef] [PubMed]
107. Singh, M.K.; Kang, C.; Ilg, P.; Crockett, R.; Kroger, M.; Spencer, N.D. Combined experimental and simulation studies of cross-linked polymer brushes under shear. *Macromolecules* **2018**, *51*, 10174–10183. [CrossRef] [PubMed]
108. Erbas, A.; Paturej, J. Friction between ring polymer brushes. *Soft Matter* **2015**, *11*, 3139–3148. [CrossRef] [PubMed]
109. Singh, M.K.; Ilg, P.; Espinosa-Marzal, R.M.; Kröger, M.; Spencer, N.D. Effect of Crosslinking on the Microtribological Behavior of Model Polymer Brushes. *Tribol. Lett.* **2016**, *63*, 17. [CrossRef]

110. Singh, M.K.; Ilg, P.; Espinosa-Marzal, R.M.; Spencer, N.D.; Kroger, M. Influence of chain stiffness, grafting density and normal load on the tribological and structural behavior of polymer brushes: A nonequilibrium-molecular-dynamics study. *Polymers* **2016**, *8*, 254. [CrossRef]
111. van der Weg, K.J.; Ritsema van Eck, G.C.; de Beer, S. Polymer brush friction in cylindrical geometries. *Lubricants* **2019**, *7*, 84. [CrossRef]
112. Munetoh, S.; Motooka, T.; Moriguchi, K.; Shintani, A. Interatomic potential for Si–O systems using Tersoff parameterization. *Comput. Mater. Sci.* **2007**, *39*, 334–339. [CrossRef]

Disclaimer/Publisher's Note: The statements, opinions and data contained in all publications are solely those of the individual author(s) and contributor(s) and not of MDPI and/or the editor(s). MDPI and/or the editor(s) disclaim responsibility for any injury to people or property resulting from any ideas, methods, instructions or products referred to in the content.